UNIVERSITY of
BRADFORD

Library

The University of Bradford Institutional Repository

http://bradscholars.brad.ac.uk

Link to publisher's version: *https://doi.org/10.14359/51689784*

Citation: Kara IF, Köroğlu MA and Ashour AF (2017) Tests of continuous concrete slabs reinforced with basalt fibre reinforced plastic bars. ACI Structural Journal. 114(05): 1201-13.

Tests of continuous concrete slabs reinforced with basalt fibre reinforced plastic bars

Ilker F. Kara; Mehmet A. Köroğlu and Ashraf F. Ashour

Ilker Fatih Kara is an Associate Professor in the Department of Civil Engineering at the Bursa Technical University, Turkey. He received his PhD in civil engineering from the University of Cukurova, Turkey. His research interests include behavior and design of reinforced concrete, hybrid steel-concrete, and fiber-reinforced concrete structures.

Mehmet Alpaslan KÖROĞLU is an Assistant Professor in the Department of Civil Engineering at Necmettin Erbakan University in Konya, Turkey. He received his BS in civil engineering from Gaziantep University, Turkey; his MS and PHD in civil engineering from Selcuk University, Turkey. His research interests include the seismic behavior and design of reinforced concrete, hybrid steel-concrete, and fiber-reinforced concrete structures.

Ashraf F. Ashour is a Professor of structural engineering at the University of Bradford, UK. He received his BSc and MSc from Mansoura University, Egypt, and his PhD from Cambridge University, UK. His research interests include shear, plasticity, and optimization of reinforced concrete structures; fiber-reinforced composites; and sustainable construction materials.

Abstract

This paper presents experimental results of three continuously supported concrete slabs reinforced with basalt-fibre-reinforced polymer (BFRP) bars. Three different BFRP reinforcement combinations of over and under reinforcement ratios were applied at the top and bottom layers of continuous concrete slabs tested. One additional concrete continuous slab reinforced with steel bars and two simply supported slabs reinforced with under and over BFRP reinforcements were also tested for comparison purposes. All slabs sections tested had the same width and depth but different amounts of BFRP reinforcement. The experimental results were used to validate the existing design guidance for the predictions of moment and shear capacities, and deflections of continuous concrete elements reinforced with BFRP bars. The continuously supported BFRP reinforced concrete slabs illustrated wider cracks and larger deflections than the control steel reinforced concrete slab. All continuous BFRP reinforced concrete slabs exhibited a combined shear–flexure failure mode. ACI 440-1R-15 equations give reasonable predictions for the deflections of continuous slabs (after first cracking) but stiffer behaviour for the simply supported slabs, whereas CNR DT203 reasonably predicted the deflections of all BFRP slabs tested. On the other hand, ISIS-M03-07 provided the most accurate shear capacity prediction for continuously supported BFRP reinforced concrete slabs among the current shear design equations.

Keywords: Reinforced concrete; Basalt reinforced polymer; Continuous slab; Shear failure; Flexural failure; Cracking.

INTRODUCTION

Corrosion of steel reinforcement constitutes one of the major problems that shorten the lifetime serviceability of concrete structures. Many steel-reinforced concrete structures exposed to deicing salts and marine environments require extensive and expensive maintenance. The use of fiber-reinforced polymer (FRP) as an alternative reinforcement in

concrete structures has emerged as an innovative solution to the corrosion problem of steel reinforcement. Applications of FRP bars, however, are not only limited to cases where corrosion is the main concern but FRP reinforcement can also be used as primary reinforcements for concrete members where magnetic transparency is required. In addition to these superior properties, FRP bars have higher strength, but lower modulus of elasticity than steel, and exhibit linear stress–strain response up to failure. The lower modulus of elasticity of FRP causes a substantial decrease in the stiffness of FRP reinforced concrete members after cracking and, consequently, higher levels of deflections under service conditions. Hence, the design of FRP reinforced concrete members is generally governed by serviceability requirements.

Over the last two decades, extensive research programs have been conducted to investigate the flexural behaviour of simply supported concrete beams and one way concrete slabs reinforced with different types of FRP reinforcing bars (Benmokrane et al. 1996; Al-Sayed 1998; Masmoudi et al. 1998; Theriault and Benmokrane 1998; Park and Naaman 1999; Pecce et al. 2000; Toutanji and Saafi 2000; Vijay and GangaRao 2001; Pilakoutas et al. 2002; Salib et al. 2002; Thiagarajan 2003; Yost et al. 2003; Rasheed et al. 2004; Ashour 2006; Kara and Ashour 2012). Various proposals for design guidelines have arisen from these studies. On the other hand, continuous reinforced concrete members are commonly used in structures such as parking garages and bridges exposed to de-icing salts, but relatively limited experimental investigations (Grace et al. 1998; Ashour and Habeeb 2008; Habeeb and Ashour 2008; El-Mogy et al. 2010; El-Mogy 2011; Mahroug et al. 2014a&b) have been carried out on continuous FRP reinforced concrete structures. However, there are concerns about the ability of FRP-reinforced continuous members to redistribute moments due to the linear elastic behavior of FRP until failure.

Grace et al (1998) reported that continuously supported T-section concrete beams reinforced with different combinations of longitudinal reinforcing bars and stirrups made of glass FRP (GFRP) and carbon FRP (CFRP) demonstrated the same load capacity as steel reinforced concrete beams but lower ductility and different failure modes. Continuously supported FRP reinforced concrete beams tested by Ashour and Habeeb (2008), and Habeeb and Ashour (2008) exhibited a small amount of moment redistribution, whereas El-Mogy et al. (2010) reported that moment redistribution in continuous FRP reinforced concrete beams is possible if the reinforcement configuration is suitably selected. More recently, Mahroug et al. (2014a&b) concluded that continuous CFRP and BFRP reinforced concrete slabs developed earlier and wider cracks and larger deflections compared with the counterpart steel reinforced concrete slab. It was also observed that combined shear and flexural failure was the dominant mode of failure for all continuous FRP reinforced concrete slabs tested. These investigations also showed that ACI 440 1R-06 equations can reasonably predict the load capacity and deflection of simply supported GFRP beams but significantly underestimate deflections of continuously supported FRP reinforced concrete beams after first cracking.

This paper presents test results of three continuously and two simply supported concrete slabs reinforced with BFRP bars and a control continuous concrete slab reinforced with steel bars. The experimental results of all slabs tested have been compared and evaluated based on modes of failure, cracking pattern, deflections, and moment redistribution. In addition, the test results were also compared with the FRP design guidance available in the literature for moment and shear capacities, and deflection to assess their accuracy.

RESEARCH SIGNIFICANCE

Although continuous reinforced concrete members are commonly used in structures, the experimental investigations on continuous FRP reinforced concrete slabs are very limited compared with simply supported ones. The current investigation presents test results of continuous BFRP reinforced concrete slabs and compares their behaviour against continuous

steel reinforced concrete slabs and simply supported BFRP reinforced concrete slabs. The experimental results of continuous and simply supported BFRP reinforced concrete slabs are employed to validate the existing design guidance and would contribute to future design development for continuous concrete elements reinforced with FRP bars.

EXPERIMENTAL INVESTIGATION

Test specimens

The experimental program consisted of testing three continuously and two simply supported BFRP reinforced concrete slabs as well as a reference continuous steel reinforced concrete slabs under mid-span point load. The continuously supported slabs had two equal spans of 1750 mm (68.9 in) each, whereas the simply supported slabs had a single span of 1750 mm (68.9 in) as shown in Figs. 1 and 2, respectively. All slabs were 500 mm (19.7 in) in width and 125 mm (4.92 in) in depth, and a 25 mm (0.98 in) thickness concrete cover for all reinforcement.

The longitudinal reinforcement details of all slabs, including the reinforcement ratio ρ_f are given in Table 1. The amount of BFRP reinforcing bars was selected to provide two different modes of flexural failure, namely BFRP bar rupture and concrete crushing. The former was accomplished by using a reinforcement ratio ρ_f (= A_f/bd, where A_f is the area of FRP reinforcing bars, b and d are the slab width and effective depth) less than the balanced reinforcement ratio ρ_{fb} (under-reinforced case), while the latter by using a reinforcement ratio greater than ρ_{fb} (over-reinforced case), where ρ_{fb} as defined in the ACI 440.1R–15 guidelines and calculated in Table 1. The slab CB-125–UO was reinforced with three BFRP longitudinal bars of 7 mm diameter (0.28 in) (under reinforcement; $\rho_f/\rho_{fb}=0.96$) on the bottom side and three 12 mm (0.47 in) diameter BFRP bars (over reinforcement) on the top side. On the other hand, the bottom reinforcement of slabs CB-125–UU and CB-125–OO was the same as the top reinforcement; three BFRP bars of 7 mm (0.28 in) diameter (under reinforcement;

$\rho_f/\rho_{fb}=0.96$) and three BFRP bars of 12 mm (0.47 in) diameter (over reinforcement) were used in CB-125–UU and CB-125–OO slabs, respectively. The simply supported slabs, SB-125–O and SB-125–U, were reinforced with three BFRP bars of 12 mm (0.47 in) diameter (over reinforced) and three BFRP bars of 7 mm (0.28 in) diameter (under reinforced; $\rho_f/\rho_{fb}=0.96$), respectively, at the bottom side. Furthermore, slab CS-125–UU was reinforced with three steel bars of 10 mm (0.394 in) diameter (under reinforced) on both the bottom and top sides to achieve a typical ductile failure mode by yielding of steel reinforcement first, followed by concrete crushing. This was accomplished by using a steel reinforcement ratio ρ_s (= A_s/bd, where A_s is the area of steel reinforcing bars) less than the balanced steel reinforcement ratio ρ_{sb} as defined in ACI 318-14. The amount of steel reinforcement in slab CS-125–UU was selected to have nearly a similar tensile capacity to that used in slab CB-125–UU. In all continuous slabs, top reinforcing bars were curtailed beyond the mid-span point load, whereas bottom bars continued throughout the slab length as shown in Fig. 1.

The nomenclature of test specimens was defined based on the amount and type of reinforcement, support system and slab thickness. The first character in the slab notation corresponds to the supporting system, 'C' for continuously supported slabs and 'S' for simply supported slabs. The second character represents the type of reinforcement, either 'B' or 'S' for BFRP and steel reinforcement, respectively. The third part of the notation reflects the slab thickness, 125 mm (4.92 in) for all slabs. The fourth character indicates the reinforcement ratio at the bottom mid-span region of the simply or continuously supported slab, namely 'U' for under-reinforcement or 'O' for over-reinforcement ratio. The last character, 'U' or 'O', is used only for the continuously supported slabs, illustrating the over middle-support reinforcement ratio. For example, the slab notation CB-125–UO indicates a continuously supported slab reinforced with BFRP bars having under and over reinforcement ratios of BFRP bars at the mid-span and over middle-support regions, respectively.

Material properties

The BFRP bars used in the slabs were manufactured by the pultrusion process where tightly packed tows of basalt fibres, impregnated with epoxy resins, are pulled through a shaped die to form highly aligned, continuous sections of BFRP bars. After resin curing, the bar surface was sand-coated to enhance the bond and force transfer between reinforcing bars and concrete. The cross-sectional properties were obtained by immersion (water displacement) testing in accordance with the ACI440.3R-04 (2004) as presented in Table 2. The mechanical characteristics of BFRP bars were obtained by carrying out tensile tests on three specimens of each bar diameter in accordance with the ACI440.3R-04. The BFRP specimen ends were embedded into steel pipes filled with expansive grout to avoid premature failure of BFRP bars at the steel jaws of the testing machine. All prepared BFRP bar specimens were tested using a 500 kN (112.4 kips) capacity universal testing machine. Table 2 shows the mechanical properties of BFRP and steel bars used.

The slabs were constructed using ready-mixed, normal weight concrete with a target compressive strength of 50 MPa (7.25 ksi) at 28 days. Table 1 lists the cube compressive strength of concrete, f_{cu}, based on the average values from testing five cubes (100 mm (3.94 in)) after testing of each slab. After concrete casting, all specimens were covered with polyethylene sheets to keep down moisture loss at all times during the period of curing and stored in the laboratory under the same condition until the day of testing.

Test setup and instrumentations

Each continuous slab comprised two equal spans supported on a roller support at each end, in addition to a hinge support at the middle as depicted in Fig. 1 and each span was loaded at its mid-point. The simply supported slabs were similarly loaded at its midspan and supported on a roller support at one end and a hinge support at the other end as shown in Fig. 2. Two load cells were used to measure the reactions at one end support, and at the main applied load from

the hydraulic ram. In order to measure the deflection of slabs, linear variable differential transformers (LVDTs) at the two mid-spans of continuously supported slabs and the mid-span of simple slabs were installed as shown in Figs. 1 and 2, respectively. In addition, two LVDTs were located at equal spacing of *L/4* on one span of the continuous slabs and the span of simple slabs to measure the deflections at these locations, where *L* is the span length. Two additional LVDTs were used at the end supports of continuous slabs to detect any movement at supports that might take place during the loading process, which could affect slab deflections and reaction distribution. The load was applied to the slabs monotonically till failure with a load-controlled rate of 5 kN/min (11.24 kips/min). The load cell and LVDT readings were automatically registered at each load increment of 5 kN (1.124 kips) using a data logger.

TEST RESULTS AND DISCUSSION

Cracking pattern and crack width

Table 3 presents the first visible cracking load of each slab tested. The steel reinforced concrete slab clearly exhibited a higher first cracking load than slabs reinforced with BFRP owing to the higher axial stiffness of steel bars than that of BFRP bars. Generally, the first crack in the BFRP continuously supported slabs was observed in the sagging moment region, followed immediately by a crack in the hogging moment region. The amount of BFRP reinforcement at different locations for the tested slabs does not have a significant effect on the first cracking load.

The crack patterns at failure in the BFRP continuously supported slabs were sketched in Fig. 3. The bold line crack in Fig. 3 indicates the major crack caused the slab failure. Slab CB-125–OO demonstrated lower crack spacings at mid-span and middle support regions than these of other BFRP continuously supported slabs due to the higher flexural reinforcement ratio at mid-span and middle support regions of slab CB-125–OO. Slabs CB-125–UU and

CB-125–UO exhibited deeper cracks at mid-span regions than slab CB-125–OO as they were under reinforced at mid-span region. In general, the number and depth of cracks for all slabs reinforced with BFRP bars were clearly larger than these of the slab reinforced with steel due to the lower elastic modulus of BFRP bars than that of steel bars.

The main crack width at both mid-span and middle support regions for all slabs are presented in Figs. 4 and 5, respectively. The control steel reinforced concrete continuous slab CS-125–UU had less crack width at both mid-span and middle support regions among all slabs before yielding of steel owing to the higher axial stiffness of steel reinforcement than that of BFRP reinforcement. As can be observed from Figs. 4 and 5, the crack width increased significantly in slab CS-125-UU after steel yielding, signifying the formation of plastic hinges. Wider cracks at the mid-span region were observed in slabs CB-125–UU and CB-125–UO with under reinforcement ratio than the over reinforced BFRP slab, CB-125–OO at their mid-span regions.

Various codes of practices (ACI440.1R-15; CSA S806-12) impose a crack width limitation varying between 0.5 and 0.7mm (0.02 and 0.028 in) at the serviceability limit state for aesthetic reasons. However, the crack width limit could be narrower in structures in aggressive environments or where water tightness is required. Figs. 4 and 5 show that the loads corresponding to the crack width limit of 0.7mm (0.028 in) varied between around 0.44 to 0.65 of the slab ultimate load with over reinforced sections showing a higher ratio than under-reinforced ones.

General behaviour and failure modes

During the testing of all continuous slabs, it was observed that first cracks were always vertical flexural cracks at either mid-span or middle support region. New additional cracks developed while existing ones propagated vertically towards the compression zone up to approximately 50% of the failure load, then the rate of formation of new cracks was

significantly reduced at higher loading stages. At this stage, existing cracks grow wider and deeper and propagated in form of diagonal shear cracks close to the middle support region. The BFRP reinforced concrete slab failure eventually occurred due to the combined flexural-shear or rupture of BFRP bars. Table 3 lists the mode and location of failure observed for each test specimens. Three different failure modes defined as combined flexural-shear failure, conventional ductile flexural failure and BFRP bar rupture were observed in the experimental tests as shown in Figs. 3 and 6, and explained below.

The combined-flexural shear failure occurred in BFRP slabs CB-125–OO, CB-125–UU, CB-125–UO and SB-125-O. This mode of failure is similar to that observed in BFRP continuous slabs tested by Mahroug et al. (2014a). The failure started at the compression side of the middle support region, followed by a major, sudden diagonal shear crack at the same location for continuous slabs CB-125–OO, CB-125–UO and CB-125–UU as shown in Fig. 3. As the load was increased for the slab CB125–UU, wide cracks propagated diagonally toward the middle support, which led to the rupture of BFRP bars at this section. The shear failure also occurred near the mid-span region propagated towards the loading point in case of the simply supported SB-125–O slab as presented in Fig. 6(a). This is mainly attributed to the low modulus of elasticity of BFRP that significantly reduces the shear resistance of the BFRP slabs tested (Mahroug et al. 2014a).

The steel reinforced concrete slab CS-125–UU demonstrated a conventional ductile flexural failure as shown in Fig. 3. The failure occurred due to yielding of tensile steel reinforcement followed by concrete crushing at mid-span region. Hogging flexural failure was also observed as a result of the yielding of the tensile steel reinforcement at the central support earlier than that at the slab mid-span.

BFRP bar rupture occurred in the simply supported slab SB-125–U, which was provided with an under reinforcement ratio ($\rho_f/\rho_{fb}=0.96$) of BFRP bars at the bottom layer, before crushing

of concrete as shown in Fig. 6(b). It was also noticed that rupture of BFRP bars was sudden and accompanied by a loud noise indicating a rapid release of energy and a complete loss of load capacity.

Load capacity

The total failure loads (the two mid-span loads in case of continuous slabs) of the tested slabs are presented in Table 3. The failure load of simply supported slab SB-125–O, which had higher reinforcement ratio at mid-span region, was around 35% of the total failure load of slabs CB-125–OO. On the other hand, the failure load of under reinforced simply supported slab SB-125–U was nearly 36% and 47% of that of slabs CB-125–UO and CB-125–UU, respectively. Furthermore, slab SB-125–U failed at 67% of the failure load of slab SB-125–O. Slab CB-125–OO that was over reinforced at both the mid-span and middle support regions tolerated more load than slab CB-125-UO that is over reinforced in the middle support region and under-reinforced at the mid-span region. In spite of the under-reinforcement ratio used at the middle support and mid-span regions of steel reinforced concrete continuous slab CS-125–UU, this slab exhibited a higher load capacity than that of slabs CB-125–UU and CB-125–UO.

Although the reinforcement ratio in slab CB-125–UO was around 2.95 times that in slab CB-125–UU over the middle support, slab CB-125–UO accomplished a failure load 30% higher than that of CB-125–UU as both failed in combined shear and flexure mode. This indicates that the top BFRP reinforcement at middle support region had less effect than that at mid-span, bottom region in enhancing the slab load carrying capacity due to the limited moment redistribution, agreeing with previous investigations on continuous FRP reinforced concrete beams (Ashour and Habeeb 2008; Habeeb and Ashour 2008; Mahroug et al. 2014a).

Failure load and moment predictions

11

Table 4 lists the experimental and predicted moment capacities of the slabs tested, where the predicted moment capacities of BFRP and steel reinforced slabs were computed according to ACI 440.1R–15 and ACI 318-14, respectively. The measured end support reaction and mid-span point load at failure of each continuous slab were used to calculate the experimental failure moment at mid-span and middle support region. Comparing the section reinforcement ratio when ρ_f against the balanced reinforcement ratio ρ_{fb}, obtained from Eq. (1) below, the moment capacity M_{pre} of mid-span and over middle support sections predicted by the ACI 440.1R–15 may be estimated from Eqs. (2) and (3) when $\rho_f > \rho_{fb}$ (over-reinforced section), and Eqs. (4) and (5) when $\rho_f < \rho_{fb}$ (under-reinforced section):

$$\rho_{fb} = 0.85\,\beta_1 \frac{f_c{'}}{f_{fu}} \frac{E_f \varepsilon_{cu}}{E_f \varepsilon_{cu} + f_{fu}} \tag{1}$$

$$M = \rho_f f_f \left(1 - 0.59 \frac{\rho_f f_f}{f_c^{'}}\right) bd^2 \tag{2}$$

$$f_f = \sqrt{\frac{(E_f \varepsilon_{cu})^2}{4} + \frac{0.85 \beta_1 f_c^{'}}{\rho_f} E_f \varepsilon_{cu}} - 0.5 E_f \varepsilon_{cu} \le f_{fu} \tag{3}$$

$$M = A_f f_{fu} \left(d - \frac{\beta_1 c_b}{2}\right) \tag{4}$$

$$c_b = \left(\frac{\varepsilon_{cu}}{\varepsilon_{cu} + \varepsilon_{fu}}\right) d \tag{5}$$

where ρ_f ($= A_f/bd$) is the FRP reinforcement ratio; A_f is the area of FRP reinforcement; b and d are the width and effective depth of the BFRP reinforced concrete slab; $f_c{'}$ is the cylinder compressive strength of concrete; f_{fu} is the ultimate tensile strength of FRP bars; ε_{cu} is the ultimate strain in concrete; E_f is the modulus of elasticity of FRP bars; f_f is the FRP stress at which concrete crushing failure mode occurs as defined in Eq. (3); c_b is the neutral axis depth for balanced failure as defined in Eq. (5); ρ_{fb} is the balanced FRP reinforcement ratio as

defined Eq. (1); and β_1 is a strength reduction factor taken as 0.85 for concrete strength up to and including 27.6 MPa. For strength above 27.6 MPa, the factor β_1 is reduced continuously at a rate of 0.05 for every 6.9 MPa of strength in excess of 27.6 MPa, but is not taken less than 0.65.

The ACI 440.1R–15 equations reasonably predicted the failure moments of the simply supported slabs SB-125–U and SB-125–O as depicted from Table 4. On the other hand, for the continuously supported BFRP reinforced concrete slabs, the ACI 440.1R-15 equations have mostly overestimated the moment capacity of mid-span sections as it is adversely affected by the existence of shear stresses participated in the failure process.

Based on the brittle nature of BFRP bars and concrete, the predicted failure load P_{pre} of the continuous BFRP reinforced concrete slabs is obtained from the lower load achieving the moment capacity at either middle support ($M_h = 0.188P_{pre}L$) or mid-span ($M_s = 0.156P_{pre}L$) section, where M_s and M_h are the moment capacities at mid-span and middle support sections calculated from the ACI 440.1R–15 equations as explained above and L is the slab span. On the other hand, the flexural load capacity P_{pre} of the steel reinforced concrete continuous slab on each span is calculated from Eq. (6) below, based on a collapse mechanism with plastic hinges at both midspan and middle support sections as the slab was under-reinforced and exhibited ductile failure mode:

$$P_{pre} = 2\left(\frac{2M_S + M_h}{L}\right) \tag{6}$$

Moreover, the failure load of the simply supported BFRP reinforced concrete slabs is estimated by satisfying the equilibrium condition at the mid-span critical section ($P_{pre} = 4M_s/L$, where M_s is the moment capacity calculated using ACI 440.1R–15, L is the slab span). A comparison between the predicted and experimental load capacities of the reinforced concrete slabs tested is presented in Table 4. The ratio of the experimental to predicted failure loads for the three continuously supported BFRP reinforced concrete slabs ranged between

0.88 and 1.07 when either the hogging or sagging section reaches the moment capacity. Overall, the load predictions were in much better agreement with the measured failure loads of all continuous slabs tested than the moment capacity predictions of the mid-span and over support sections as it was calculated based on the lower load achieving the moment capacity at either middle support or mid-span section.

Load and moment redistribution

Fig. 7 presents the measured end support reaction versus the total applied load for each continuous slab tested. To assess the load redistribution, the elastic reaction at the end support, considering uniform flexural stiffness throughout the entire length of slabs, is also illustrated in Fig. 7. At the initial stages of loading before concrete cracking, the measured end support reaction of continuous slabs was very close to that obtained from the elastic analysis due to the linear elastic characteristics of concrete, BFRP bars and steel bars before reaching the cracking load. The end support reaction for slab CB-125–UO was the smallest in all slabs tested due to the higher stiffness at middle support region and cracks at the mid-span region, indicating signs of load distribution from the mid-span region to the middle support region. Slabs CB-125–OO and CB-125–UU having a similar flexural rigidity along the slab spans demonstrated a slight load redistribution due to the mid-span cracks, as the end support reaction was slightly reduced in comparison with the elastic end support reaction.

Figs. 8(a-c) present the experimental and elastic bending moment distributions at failure along one span of the continuous BFRP slabs tested. The bending moments of the continuous slabs tested were determined from the monitored reaction and applied load according to equilibrium condition. The predicted moment capacities at both mid-span and over support sections calculated from the ACI 440.1R–15 are also plotted in Fig. 8. In order to evaluate the amount of moment redistribution, β_{rd}, the following expression is used:

$$\beta_{rd} = \frac{M_{exp} - M_e}{M_e} \ x \ 100\% \tag{7}$$

where M_{exp} is the bending moment obtained from experiments using the measured end support reaction and mid-span load, and M_e is the bending moment calculated from elastic analysis at failure load.

The amounts of moment redistribution, β_{rd}, for the mid-span and over support sections are also given in Fig. 8. As can be observed from Figs. 8(a-c), the experimental bending moment distribution is different from that obtained from linear elastic analysis at failure load for all continuous BFRP slabs. The moment redistribution percentage β_{rd} is always higher than that of mid-span sections for all BFRP continuous slabs tested. The highest moment redistribution at mid-span (24%) and over middle support sections (40%) occurred in slab CB-125–UO. Figs. 8(a-c) also show that no mid-span section of the tested slabs reached the corresponding moment capacity as predicted by the ACI 440.1R–15. Overall, the moment redistribution occurred is likely to be attributed to cracks at different locations.

Table 4 presents the moment redistribution factor β_{rd} for the sagging and hogging moments at mid span and over the middle support of continuous BFRP and steel reinforced concrete slabs. The ratio α between the hogging and sagging moment redistributions for the tested slabs is also given in Table 4. The value of α seems very similar for all tested slabs as also obtained in previous studies on continuous slabs (Mahroug et al. 2014a&b). Kara and Ashour (2013) presented an elastic analysis for two span continuous elements under mid-span point load and showed that the hogging moment redistribution should always be 66% more than the sagging moment redistribution, confirming the moment redistribution factor β_{rd} obtained in the current experimental investigation.

Load–deflection response

The experimental mid-span point load against the recorded mid-span deflection curves of all slabs are shown in Fig. 9. The LVDT at the end supports did not record any noticeable movement; therefore not presented. For continuous slabs, the recorded mid-span deflections at

one side were similar to those at the other side, therefore, one side mid-span deflections are shown in Fig. 9. At initial stages of loading, all slabs were un-cracked and they exhibited linear load deflection behaviour owing to the linear elastic characteristics of concrete before cracking and BFRP bars, as well as steel bars before reaching the yielding point. As the load increased, the slab axial stiffness, E_fA_f, is further reduced due to the occurrence of more cracks. As expected, the steel reinforced concrete continuous slab CS-125–UU exhibited the lowest deflection among all slabs before yielding of steel owing to the higher axial stiffness of steel bars. Generally, the amount of BFRP reinforcement is a key factor in enhancing the flexural stiffness and, consequently, reducing deflections of the tested slabs. For example, slab CB-125–UO demonstrated higher deflection than CB-125–OO as the mid-span flexural stiffness of slab CB-125–OO is higher than that of CB-125–UO. The simply supported slab SB-125-O deflected less than the slab SB-125-U as the bottom BFRP reinforcement used in slab SB-125-O had higher stiffness than that of the bottom BFRP bars in slab SB-125-U. The slab SB-125-U also showed unacceptable large deflection at failure compared with its span (>L/17) as indicated in Fig. 9.

Fig. 10 shows the deflection curve of continuous slabs, measured at 3 points along the slab span at a mid-span point load of 30 kN (6.74 kips). Fig. 10 shows that the highest deflection among all continuous slabs occurred in slab CB–125-UU with the smallest amount of BFRP reinforcement at the mid-span region, whereas the lowest deflection exhibited by the steel reinforced concrete slab C–S–UU owing to the higher axial stiffness of steel reinforcement used, followed by CB–125-OO.

Prediction of mid-span deflections

In this section, two design guidelines, namely ACI 440.1R–15 (ACI 2015) and CNR DT203, are employed to predict the mid-span deflections of the slabs tested. The ACI 440 1R–15 provides a modified form of Bischoff's equation, that is the section based expression for the

effective moment of inertia, I_{eff}, to be used for computing the mid-span deflection of FRP reinforced concrete elements as in Eq. (8) below:

$$I_{eff} = \left(\frac{I_{cr}}{1 - \gamma \left(\frac{M_{cr}}{M} \right)^2 \left(1 - \frac{I_{cr}}{I_g} \right)} \right) \tag{8}$$

where M_{cr} is the cracking moment of the member cross-section, M is the applied moment, γ is a factor dependent on load and boundary conditions and suggested as $\gamma = 1.72 - 0.72\frac{M_{cr}}{M}$, $I_g(= bh^3/12)$ is the gross section moment of inertia, b and h are the width and overall depth of concrete slabs, respectively, I_{cr} $(=\left(\frac{bd^3}{3}\right)k^3 + n_f A_f d^2 (1 - k)^2)$ is the transformed cracked moment of inertia, where k $(= \sqrt{(\rho_f n_f)^2 + 2\rho_f n_f} - \rho_f n_f)$, is the ratio of the neutral axis depth to reinforcement depth, n_f $(= E_f / E_c)$ is the modular ratio of FRP reinforcement with respect to concrete and E_c $(=4750 \sqrt{f_c'})$ in N/mm^2 is the concrete modulus of elasticity. The immediate mid-span deflections of simple and continuous slabs are then calculated from the linear elastic structural analysis techniques using the effective moment of inertia of FRP reinforced elements (Eq. (8)).

The CNR DT203 (2006) design manual also suggested the following equation for immediate deflection of FRP reinforced concrete elements and slabs as follows:

$$\Delta = \Delta_1 \, \beta_1 \, \beta_2 \left(\frac{M_{cr}}{M} \right)^2 + \Delta_2 \left(1 - \beta_1 \, \beta_2 \left(\frac{M_{cr}}{M} \right)^2 \right) \tag{9}$$

where Δ_1 and Δ_2 are the deflections calculated based on the hypothesis of uncracked and cracked cross sections, respectively, β_1 and β_2 are factors depending on the concrete-FRP bond quality and duration of loading, respectively. The suggested values for β_1=0.5 for FRP reinforcement and β_2=1 for short term loading.

Figures 11 to 15 compare the experimental deflections of BFRP reinforced concrete slabs tested in the present study against the predictions obtained from the two design codes, namely ACI 440–1R–15 and CNR DT203. The deflection predictions obtained from ACI 440-1R-15 and CNR DT203 are in good agreement with the measured mid-span deflections of continuous slabs (CB-125–UO, CB-125-UU and CB-125-OO) up to failure. However, the ACI 440-1R-15 predicted stiffer behaviour for slab CB-125-UU. Meanwhile, CNR DT203 code reasonably predicted the deflections of simple slabs SB-125–O and SB-125–U, with a steady underestimation of the deflection for loads higher than 70% of each slab's failure load; however, ACI 440-1R-15 predicted slightly stiffer behaviour for the two simply supported slabs.

Shear capacity prediction

The predictions of FRP shear design provisions in current design guidelines are compared with the experimental load capacity to assess their accuracy. In addition to the experimental results presented above, test results of 10 slab specimens available in the literature (Mahroug et al. (2014a&b)) are also considered. These specimens were tested under mid-span point load and had two equal spans of 2000 mm (78.74 in) each for continuously supported slabs and a span of 2000 mm (78.74 in) for the simply supported slabs. All the materials and geometrical details of these test specimens are given in the study of Mahroug et al. (2014a&b). The predictions of the shear design equations for FRP reinforced concrete members recommended by ACI 440-1R15, CAN/CSA S806- 12, JSCE-97, ISIS-M03-07 and BISE-99 are evaluated in this study. All the material reduction factors are assigned to one in the shear design equations for comparison purposes. Table 5 presents the ratio of the experimental and predicted shear capacities of V_{exp}/V_{pred}, indicating that all the five design methods provide conservative predictions with an average value of V_{exp}/V_{pred} greater than 1 for continuous slabs. This is may be attributed to the combined flexure-shear failure, rather than a pure shear

18

failure. However, ISIS-M03-07 design method gives the most reasonable results with an average ratio of V_{exp}/V_{pred} equal to 1.21. Furthermore, the ISIS-M03-07 design guideline also shows the lowest standard deviation of 0.32 compared with 0.87 for ACI 440.1R-15, 0.46 for JSCE-97, 0.47 for CAN/CSA S806-12 and 0.36 for BISE-99 as shown in Table 5. On the other hand, the ACI 440-1R15 design method provides the most conservative predictions with a mean ratio of V_{exp}/V_{pred} of 2.73 without applying safety factor, agreeing with previous investigations reported by Salib et al. (2002). The JSCE-97 design equation also gives overly conservative with an average of V_{exp}/V_{pred} of 1.66. The CAN/CSA S806-12 and JSCE-97, however, provide much better results of a mean ratio V_{exp}/V_{pred} of 1.35 and 1.26 than that of JSCE-97 and ACI 440-1R15 design guidelines. It is to be noted that most of the current shear design provisions gives unconservative results for the simply supported concrete slabs reinforced with FRP bars as the value of V_{exp}/V_{pred} is smaller than 1.

SUMMARY AND CONCLUSIONS

This paper presented the results of testing two simply and three continuously supported concrete slabs reinforced with BFRP bars. One additional concrete continuous slab reinforced with steel bars was also tested for comparison purposes. The experimental results were also compared with the code equations for moment capacity, deflections and shear capacity. The main findings of this investigation are summarized below.

- The continuously supported BFRP reinforced concrete slabs exhibited wider cracks and larger deflections than the control steel reinforced concrete slab due to the lower elastic modulus of BFRP bars compared with steel.

- At early stages of loading before the onset of concrete cracking, the measured end support reactions of all slabs were very similar and close to that obtained from elastic analysis. After concrete cracking, the measured reactions were slightly lower than that obtained from elastic analysis.

- Combined shear and flexural failure was the dominant mode of failure for all continuous BFRP reinforced concrete slabs, indicating that shear in FRP reinforced concrete slabs is likely to contribute to the failure.

- The BFRP continuous slab with over reinforcement at both the middle support and mid span regions demonstrated the highest load capacity and lowest deflection of all BFRP slabs.

- The moment redistribution occurred is likely to be attributed to cracks at different locations.

- The ACI 440.1R-15 overestimated the experimental moment capacity of BFRP reinforced concrete slabs owing to the combined shear-flexure failure.

- The ACI 440-1R-15 reasonably predicted the deflections of continuous slabs but stiffer behaviour for the simple slabs. On the other hand, CNR DT203 reasonably predicted the deflections of all BFRP slabs.

- The ACI 440.1R-15 shear design equation gives the most conservative predictions for the shear capacity of FRP reinforced concrete slabs even though the safety factor was not considered. On the other hand, ISIS-M03-07 design method provides the most reasonable result for the shear capacity of concrete slabs reinforced with BFRP bars.

REFERENCES

American Concrete Institute (ACI), 2015, ''Guide for the design and construction of concrete reinforced with FRP bars.'' *ACI 440.1R-15*, Farmington Hills, MI 48331.

American Concrete Institute (ACI 440.3R-04), 2004, ''Guide Test methods for Fiber-Reinforced Polymers (FRPs) for reinforcing or strengthening concrete structures.'' Farmington Hills, MI.

Al-Sayed, S.H., 1998, ''Flexure behaviour of concrete beams reinforced with GFRP bars,'' *Cement and Concrete Compos*ite, 20(1), 1–11.

Ashour, A.F., 2006, ''Flexural and shear capacities of concrete beams reinforced with GFRP bars,'' *Construction and Building Materials*, 20(10), 1005–1015.

Ashour, A.F.; and Habeeb, M.N., 2008, ''Continuous concrete beams reinforced with CFRP bars,'' *Structures and Building*, 161(6), 349–357.

Benmokrane, B.; Chaallal. O.; and Masmoudi, R., 1996, ''Flexural response of concrete beams reinforced with FRP reinforcing bars,'' *ACI Structural Journal*, 93(1), 46–53.

Canadian Standards Association (CSA) (2012), ''Design and construction of building components with fibre-reinforced polymers,'' *CSA Standard S806-12*, Ont., Canada.

CNR-DT 203, 2006, ''Guide for the design and construction of concrete structures reinforced with fiber-reinforced polymer bars,'' National Research Council, Rome, Italy.

El-Mogy, M.; El-Ragaby, A.; and El-Salakawy, E., 2010, ''Flexural behaviour of FRP-reinforced continuous concrete beams,'' *Journal of Composite for Construction,* 14(6), 669–680.

El-Mogy, M., 2011, ''Behaviour of continuous concrete beams reinforced with FRP bars,'' Ph.D. Thesis, *University of Manitoba*, Winnipeg, Manitoba, Canada, 198 pp.

Grace, N.F.; Soliman, A.K.; Abdel-Sayed, G.; and Saleh, K.R., 1998, ''Behavior and ductility of simple and continuous FRP reinforced beams,'' *Journal of Composite for Construction*, 2(4), 186–194.

Habeeb, M.N.; and Ashour, A.F., 2008, ''Flexural behavior of continuous GFRP reinforced concrete beams,'' *Journal of Composite for Construction,* 12(2), 115–124.

ISIS Canada, 2007, ''Design manual 3, reinforcing concrete structures with fibre reinforced polymers (FRPs).'' ISIS Canada Corporation, the Canadian Network of Centers of Excellence on Intelligent Sensing for Innovative Structures, Winnipeg, Manitoba, Canada.

Kara, I.F.; and Ashour, A.F., 2013, "Moment redistribution in continuous FRP reinforced concrete beams," *Construction and Building Materials*, 49, 939-948.

Kara, I.F.; and Ashour. A.F., 2012, ''Flexural performance of concrete beams reinforced with fibre-reinforced polymers,'' *Composite Structures*, 94(5), 1616–1625.

Mahroug, M.E.M.; Ashour, A.F.; and Lam, D., 2014a, ''Experimental response and code modelling of continuous concrete slabs reinforced with BFRP bars,'' *Composite Structures*, 107(1), 664-674.

Mahroug, M.E.M.; Ashour, A.F.; and Lam, D., 2014b, ''Tests of continuous concrete slabs reinforced with carbon fibre reinforced polymer bars,'' *Composite Part B: Engineering*, 66(11), 348-357.

Masmoudi, R.; Thériault, M.; and Benmokrane, B., 1998, ''Flexural behavior of concrete beams reinforced with deformed fiber reinforced plastic reinforcing rods.'' *ACI Structural Journal,* 95(6), 665–676.

Park, S.; and Naaman, A., 1999, "Mathematical Model for FRP Dowels Subject to Tension and Shear Forces", The 4th International Symposium on Fiber Reinforced Polymers for Reinforced Concrete Structures, ACI SP-188, 55-63.

Pecce, M., Manfredi, G., and Cosenza, E. (2000). ''Experimental response and code models of GFRP RC beams in bending,'' *Journal of Composite for Construction,* 4(4), 182–187.

Pilakoutas, K.; Neocleous, K.; and Guadagnini, M., 2002, ''Design philosophy issues of fiber reinforced polymer reinforced concrete structures,'' *Journal of Composite for Construction*, 6(3), 154–161.

Rasheed, H.A.; Naye, I.R.; and Melhem, H., 2004, ''Response prediction of concrete beams reinforced with FRP bars,'' *Composite Structures,* 65, 193–204.

Salib, S.; Abdel-Sayed, G.; and Grace, N., 2002, "An Analytical Approach towards the Strength of Concrete Beams Reinforced and/or Prestressed with FRP Bars", *Canadian Journal of Civil Engineering (CJCE)*, 29(2), 301-315.

Theriault, M.; and Benmokrane, B., 1998, ''Effects of FRP reinforcement ratio and concrete strength on flexure behaviour of concrete beams,'' *Journal of Composite for Construction*, 2(1), 7–16.

Thiagarajan, G., 2003, ''Experimental and analytical behavior of carbon fiber-based rods as flexural reinforcement,'' *Journal of Composite for Construction*, 7(1), 64–72.

Toutanji, H.; and Saafi, M., 2000, ''Flexure behaviour of concrete beams reinforced with glass fiber-reinforced polymer (GFRP) bars,'' *ACI Structural Journal,* 97(5), 712–719.

Vijay, P.V. and GangaRao, H.V.V., 2001, ''Bending behavior and deformability of glass fibre reinforced polymer reinforced concrete members,'' *ACI Structural Journal*, 98(6), 834–842.

Yost, J.R.; Gross, S.P.; and Dinehart, D.W., 2003, ''Effective moment of inertia for glass fiber reinforced polymer-reinforced concrete beams,'' *ACI Structural Journal*, 100(6), 732–739.

List of Tables

Figure Captions List

Fig. 1 Experimental setup and details of continuously supported slabs.

Fig. 2 Experimental setup and details of BFRP simply supported slabs.

Fig. 3 Typical crack patterns and modes of failure of reinforced concrete continuous.

Fig. 4 Applied load versus crack width at mid-span of all slabs tested.

Fig. 5 Applied load versus crack width at middle support of continuous slabs tested.

Fig. 6. Failure modes of simply supported slabs tested.

Fig. 7 Total applied load versus end support reaction of continuous slabs tested.

Fig. 8 Experimental and elastic bending moment distributions at failure, and moments of resistance at critical sections of beams tested.

Fig. 9 Load–deflection at mid-span for all slabs tested.

Fig. 10 Experimental profile of deflections along continuous slabs tested at a midspan load of 30 kN (6.74 kips).

Fig. 11 Experimental and predicted deflections for slab CB-125–UO.

Fig. 12 Experimental and predicted deflections for slab CB-125–UU.

Fig. 13 Experimental and predicted deflections for slab CB-125–OO.

Fig. 14 Experimental and predicted deflections for slab SB-125–U.

Fig. 15 Experimental and predicted deflections for slab SB-125–O.

Table 1 Designation of slabs and characteristics of longitudinal reinforcement and concrete.

Slab	Longitudinal reinforcing bars								Concrete compressive strength, f_{cu} (N/mm²)
	Bottom bars at midspan				Top bars at central support				
	No	Diameter (mm)	ρ_f or ρ_s (%)	ρ_f/ρ_{fb} or ρ_s/ρ_{sb}	No	Diameter (mm)	ρ_f or ρ_s (%)	ρ_f/ρ_{fb} or ρ_s/ρ_{sb}	
CB-125-UU	3 BFRP	7	0.24	0.96	3 BFRP	7	0.24	0.96	49.6
CB-125-UO	3 BFRP	7	0.24	0.96	3 BFRP	12	0.70	2.55	51.1
CB-125-OO	3 BFRP	12	0.70	2.55	3 BFRP	12	0.70	2.55	64.1
SB-125-U	3 BFRP	7	0.24	0.96	--	--	--	--	53.4
SB-125-O	3 BFRP	12	0.70	2.55	--	--	--	--	53.4
CS-125-UU	3 Steel	10	0.49	0.16	3	10	0.49	0.163	63.5

Note: The concrete compressive strength was determined from testing 5 cubes (100x100x100 mm) for each slab specimen. The cylinder compressive strength of concrete (f_c') is assumed to be 0.85*f_{cu}. 1 MPa = 0.145 ksi, 1 mm = 0.0394 in.

Table 2 Mechanical properties of BFRP and steel reinforcing bars.

Type of bars	Bar diameter (mm)		Measured bar area (mm^2)	Modulus of Elasticity (GPa)	Tensile strength (MPa)	Ultimate strain	Yield strength (MPa)
	Nominal	Measured based on ACI-440.3R					
BFRP	7	7.47	38.48 (Nominal) 43.75 (ACI440.3R)	50	1250	0.025	N/A
BFRP	12	12.54	113.1 (Nominal) 123.4 (ACI440.3R)	50	1165	0.023	N/A
Steel	10		78.54	200	660	-	620

Note: The nominal diameter (of 7 mm and 12 mm (0.28 and 0.47 in)) were used in calculating the tensile strength, modulus of elasticity and ultimate strain of BFRP bars. 1 MPa = 0.145 ksi, 1 mm = 0.0394 in.

Table 3 First cracking and total experimental failure loads of slabs tested.

Slab Notation	First cracking loads at slab mid-span, P_{cr} (kN)		Total experimental failure load (kN)	Observed failure mode
	Sagging	Hogging		
CB-125-UO	12.00	17.00	90.14	Flexure–shear failure at middle support
CB-125-UU	15.00	15.25	69.03	Flexure–shear failure at middle support
CB-125-OO	14.00	17.50	138.76	Flexure–shear failure at middle support
CS-125-UU	26.50	18.60	113.40	Flexural–tension failure at both mid-span and middle support
SB-125-U	8.30	N/A	32.56	BFRP bar rupture at mid-span
SB-125-O	9.00	N/A	48.80	Flexure–shear failure at mid-span

Note: 1 kN = 0.2248 kips.

Table 4 Comparisons of experimental and ACI 440 moment and load capacities of slabs tested and moment redistribution at failure of continuous slabs.

Slab Notation	Experimental results			ACI predictions			$M_{exp}/M_{pred.}$		P_{exp}/P_{pre}	Moment redistribution $\beta_{rd}(=\dfrac{M_{exp}-M_e}{M_e}\times 100\%)$		α $(=(\beta_{rd})_{\text{Hogging}}/(\beta_{rd})_{\text{Sagging}})$
	Failure moment, M_{exp} (kNm)		Failure load on each span, P_{exp} (kN)	Failure moment (kN)		Failure load on each span, P_{pre} (kN)	Sagging	Hogging				
	Sagging	Hogging		Sagging	Hogging					Sagging	Hogging	
CB-125-UO	9.32	20.79	45.07	13.00	21.81	47.62	0.72	0.95	0.95	24.25	40.20	1.66
CB-125-UU	8.19	13.83	34.52	12.86	12.86	39.09	0.64	1.075	0.88	13.12	21.80	1.66
CB-125-OO	17.70	25.31	69.38	21.37	21.37	64.92	0.83	1.18	1.07	13.69	22.70	1.66
CS-125-UU	15.2	19.18	56.68	14.10	14.1	48.34	1.08	1.36	1.17	1.72	2.85	1.66
SB-125-U	14.25	N/A	32.56	13.20	N/A	30.17	1.08	N/A	1.08	-	-	-
SB-125-O	21.35	N/A	48.80	20.10	N/A	45.35	1.08	N/A	1.08	-	-	-

Note: 1 kN = 0.2248 kips; 1 mm = 0.0394 in.

Table 5 Comparison of predicted and experimental shear capacities.

Reference	Slab	Type of support condition	Experimental shear Strength (V_{exp})	ACI 440.1 R-15		BISE-99		ISIS M03-07		CSA S806-12		JSCE-97	
				V_{pred} (kN)	V_{pred}/V_{exp}	V_{pred} (kN)	V_{pred}/V_{exp}	V_{pred} (kN)	V_{pred}/V_{exp}	V_{pred} (kN)	V_{pred}/V_{exp}	V_{pred} (kN)	V_{pred}/V_{exp}
Present study	CB-125-UU	Continuously supported	25.16	10.81	2.32	27.48	0.92	31.50	0.80	34.65	0.73	20.03	1.26
	CB-125-UO	Continuously supported	34.42	10.90	3.16	27.75	1.24	31.97	1.08	35.17	0.98	20.23	1.70
	CB-125-OO	Continuously supported	50.63	19.41	2.61	43.17	1.17	35.81	1.41	39.39	1.29	30.49	1.66
Mahroug et al. (2014a)	CB-150-OO	Continuously supported	80.42	21.62	3.72	45.67	1.76	40.51	1.99	44.56	1.81	35.20	2.29
	CB-150-OU	Continuously supported	56.38	21.75	2.59	46.02	1.23	40.97	1.38	45.06	1.25	35.46	1.59
	CB-150-UO	Continuously supported	53.60	13.96	3.84	33.87	1.58	41.91	1.28	46.1	1.16	26.10	2.05
	CB-150-UU	Continuously supported	53.86	13.80	3.90	33.36	1.62	40.97	1.32	45.06	1.20	25.71	2.10
Mahroug et al. (2014b)	CC-150-OO	Continuously supported	98.63	39.41	2.50	70.96	1.39	65.63	1.50	43.61	2.26	54.68	1.80
	CC-150-OU	Continuously supported	81.67	38.70	2.11	69.47	1.18	63.57	1.29	42.25	1.93	53.54	1.53
	CC-150-UO	Continuously supported	80.04	21.95	3.65	46.06	1.74	66.47	1.20	44.17	1.81	35.50	2.26
	CC-150-UU	Continuously supported	71.44	22.06	3.24	46.33	1.54	67.05	1.07	44.56	1.60	35.70	2.00
Present study	SB-125-O	Simply supported	24.4	18.49	1.32	40.62	0.60	32.68	0.75	35.95	0.68	29.61	0.82
Mahroug et al. (2014a)	SB-150-O	Simply supported	42.8	21.89	1.96	46.39	0.92	41.46	1.03	45.60	0.94	35.75	1.19
Mahroug et al. (2014b)	SC-150-O	Simply supported	57.5	40.15	1.43	72.52	0.79	67.81	0.85	45.061	1.28	55.89	1.03
		Mean		2.74		1.26		1.21		1.35		1.66	
		SD		0.87		0.36		0.32		0.47		0.46	
		COV (%)		31.75		28.57		26.44		34.81		27.71	

Note: 1 kN = 0.2248 kips
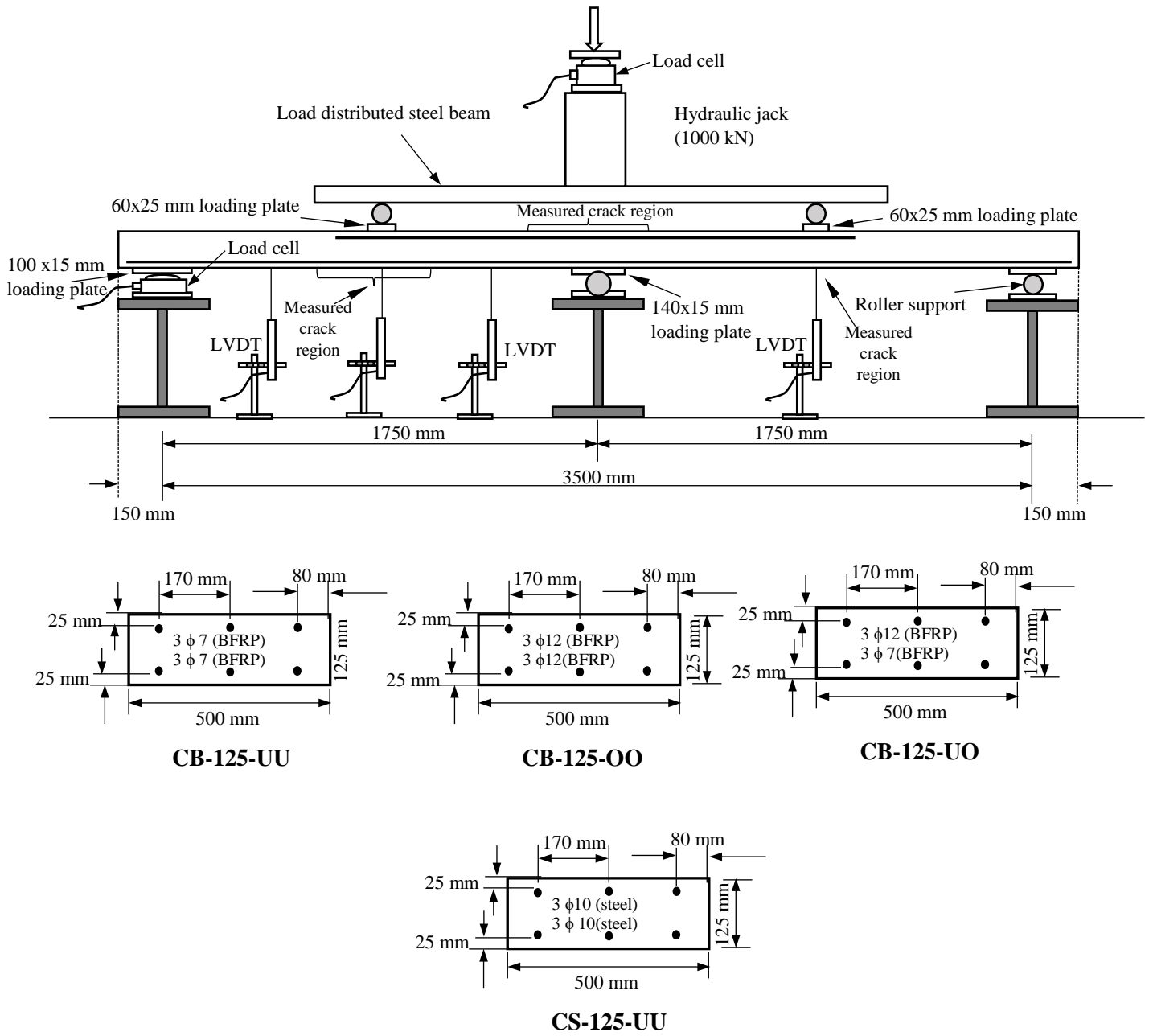
Fig. 1. Experimental setup and details of continuously supported slabs.

SB-125-U   **SB-125-O**
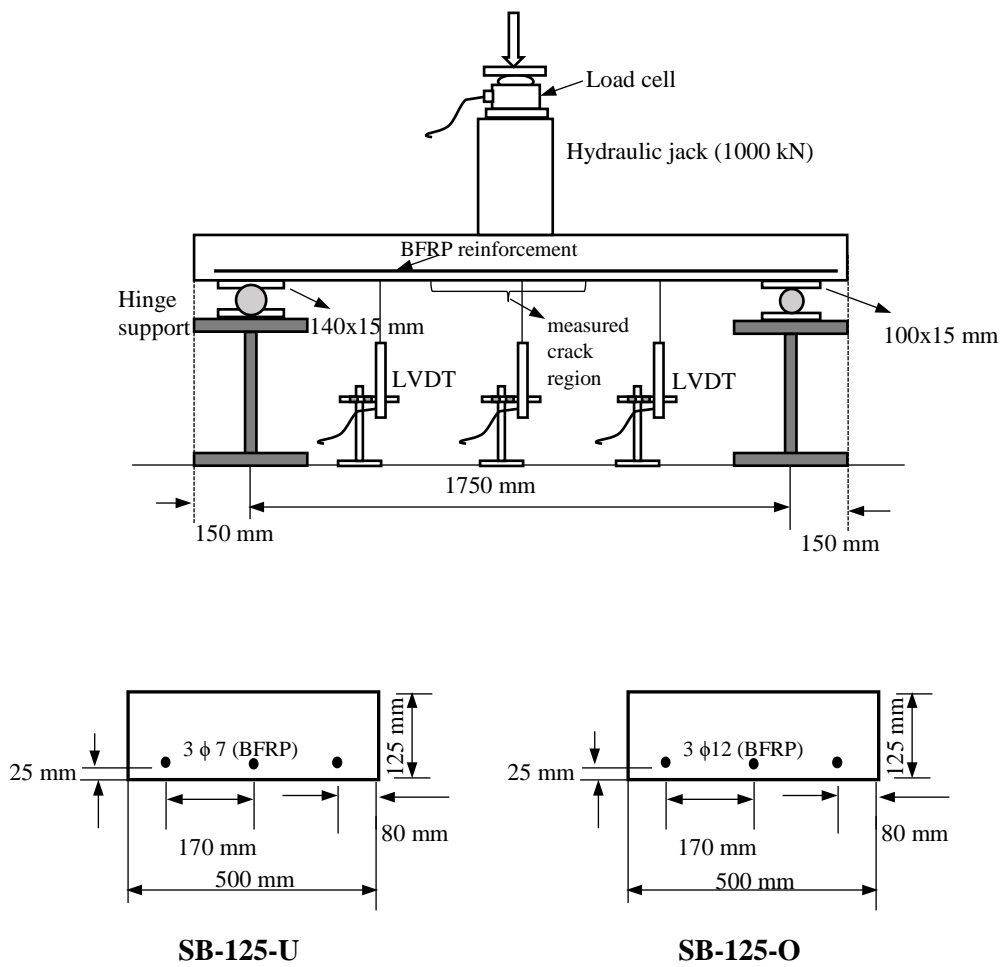
1 mm = 0.0394 in

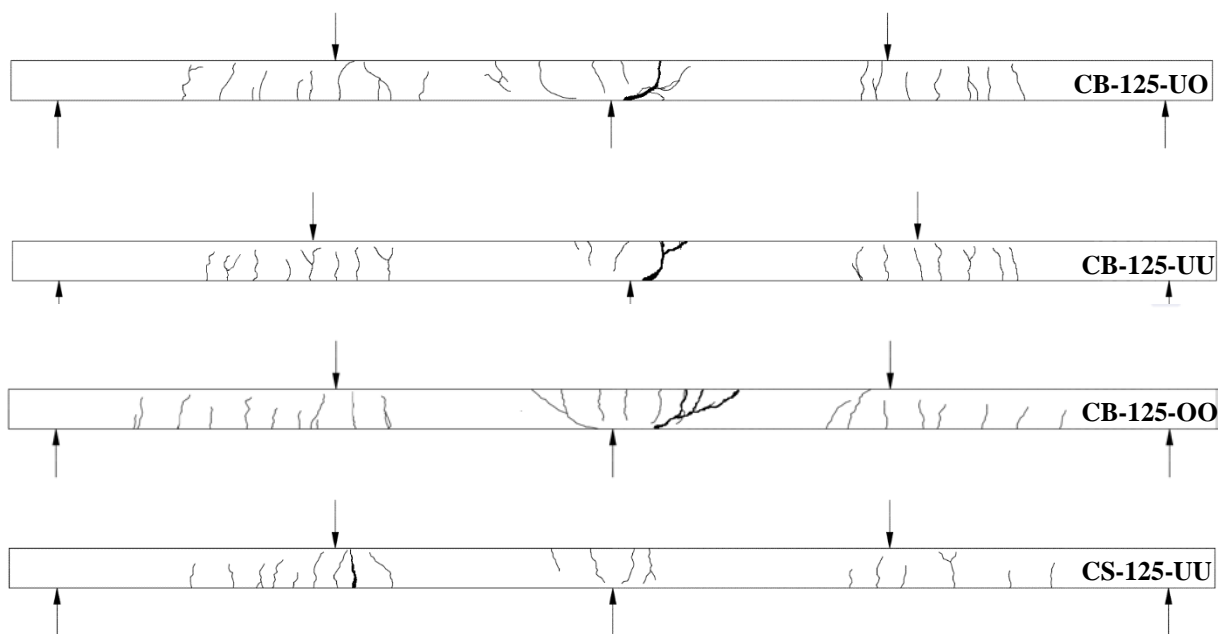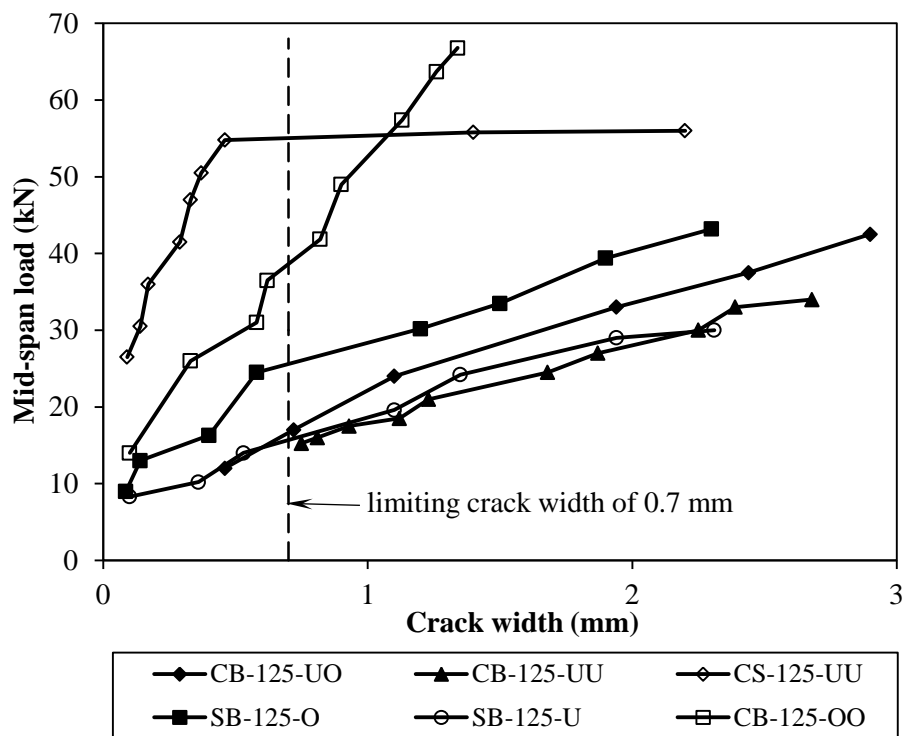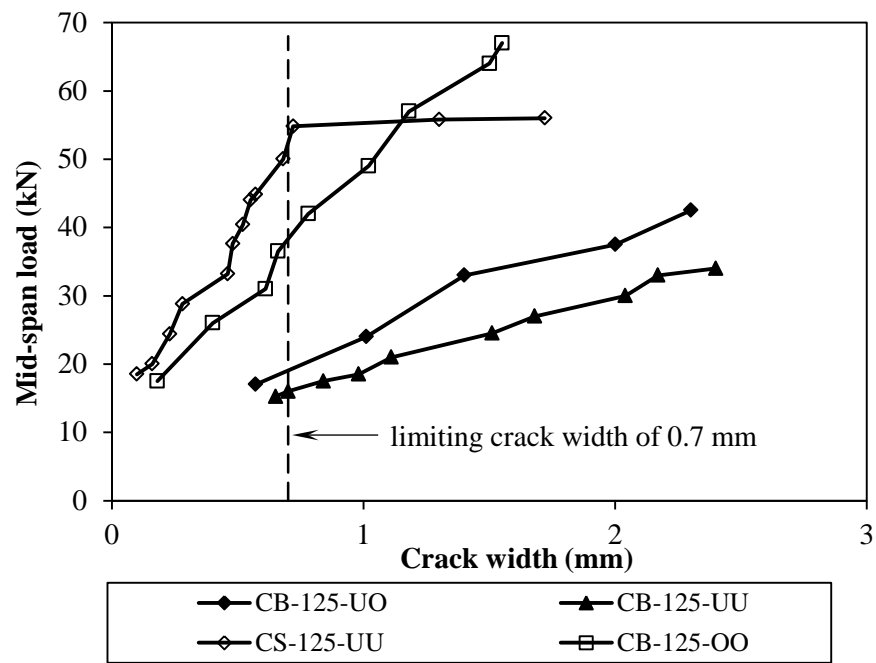**Fig. 2.** Experimental setup and details of BFRP simply supported slabs.

Fig. 3. Typical crack patterns and modes of failure of reinforced concrete continuous. slabs.

1 kN = 0.2248 kips; 1 mm = 0.0394 in

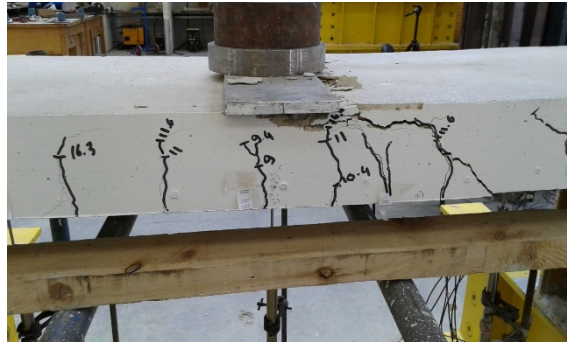**Fig. 4.** Applied load versus crack width at mid-span of all slabs tested

Fig. 5. Applied load versus crack width at middle support of continuous slabs tested

Mid span load

(a) Flexural-shear failure at midspan of SB-125-O slab

Mid span load

(b) BFRP tensile rupture failure at midspan of SB-125-U slab

Fig. 6. Failure modes of simply supported slabs tested.
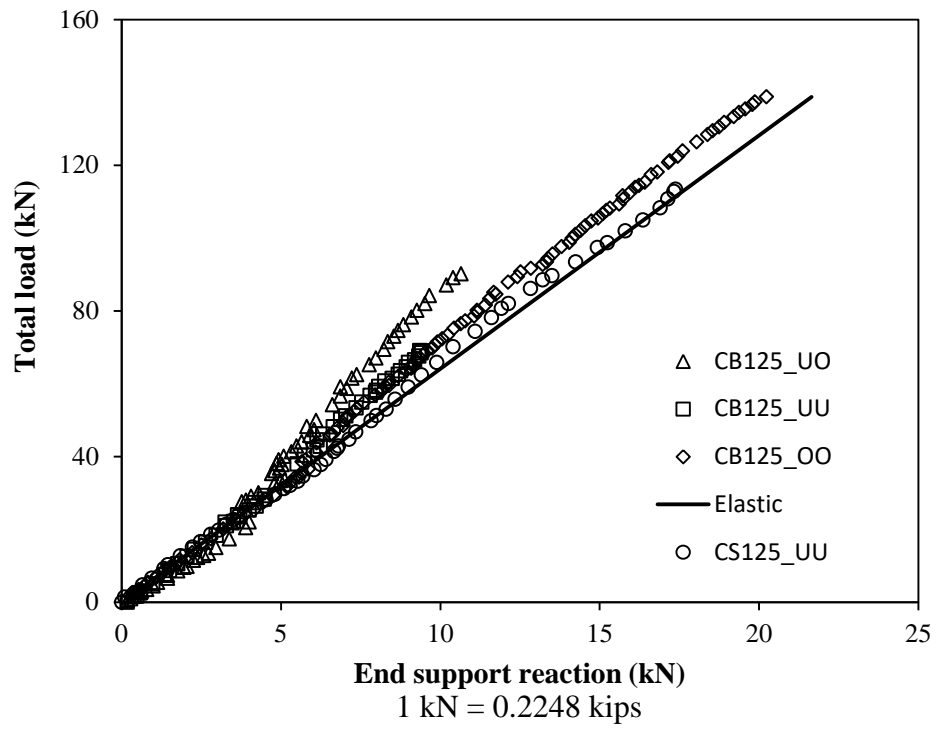
Fig. 7. Total applied load versus end support reaction of continuous slabs tested.
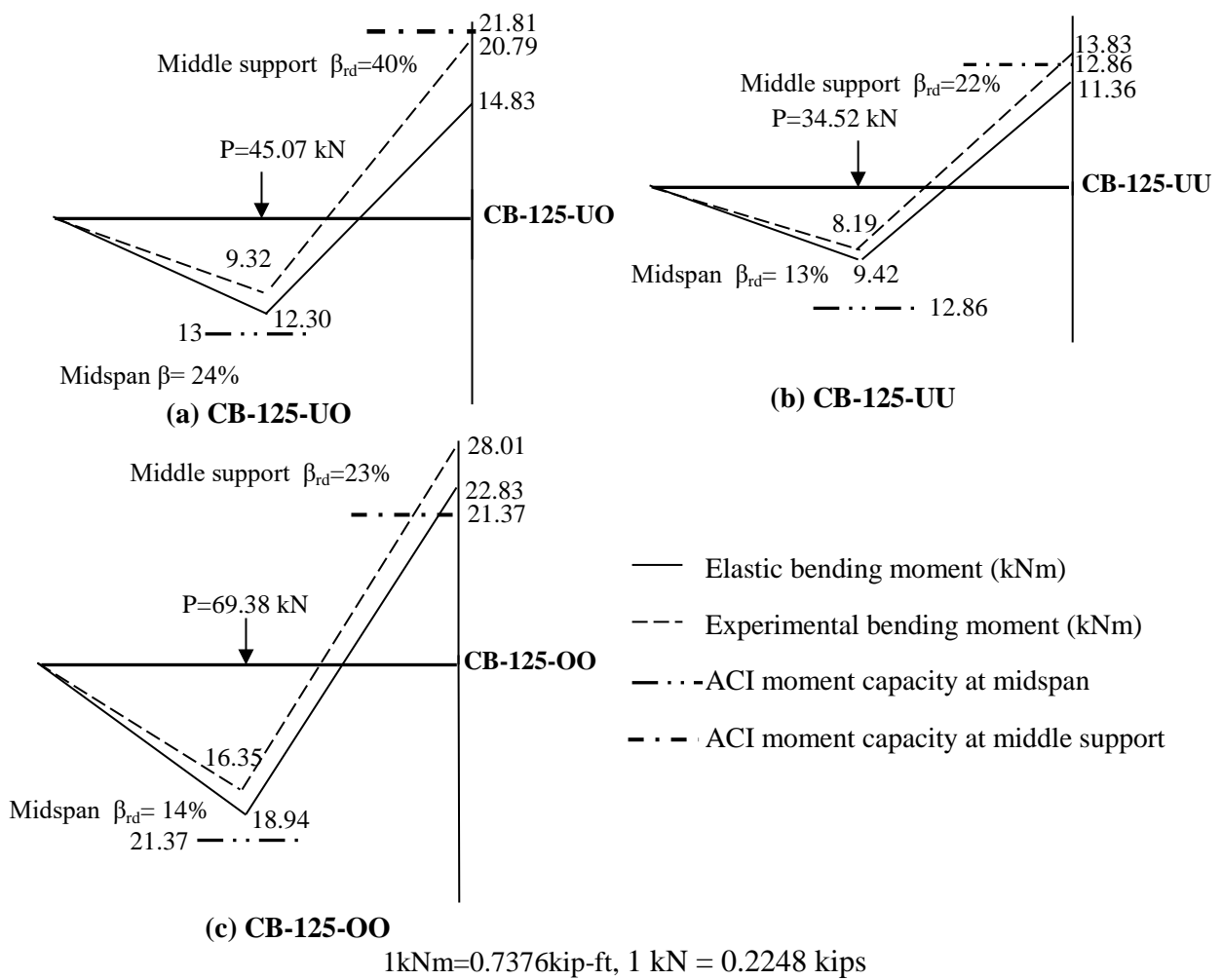
Fig. 8. Experimental and elastic bending moment distributions at failure, and moments of resistance at critical sections of beams tested.
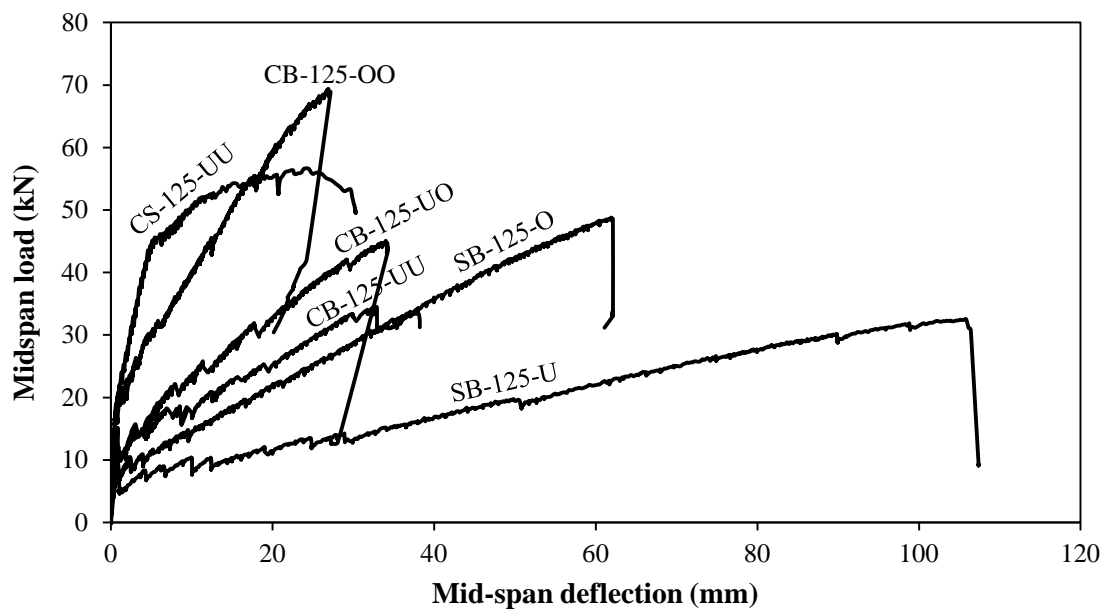
1 kN = 0.2248 kips; 1 mm = 0.0394 in
Fig. 9. Load–deflection at mid-span for all slabs tested.
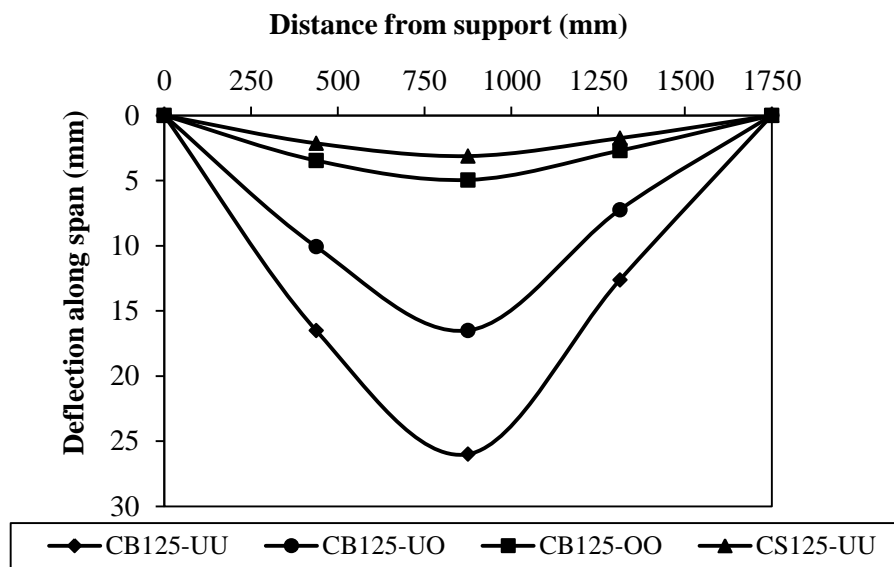
Fig. 10. Experimental profile of deflections along continuous slabs tested at a midspan load of 30 kN (6.74 Kips).
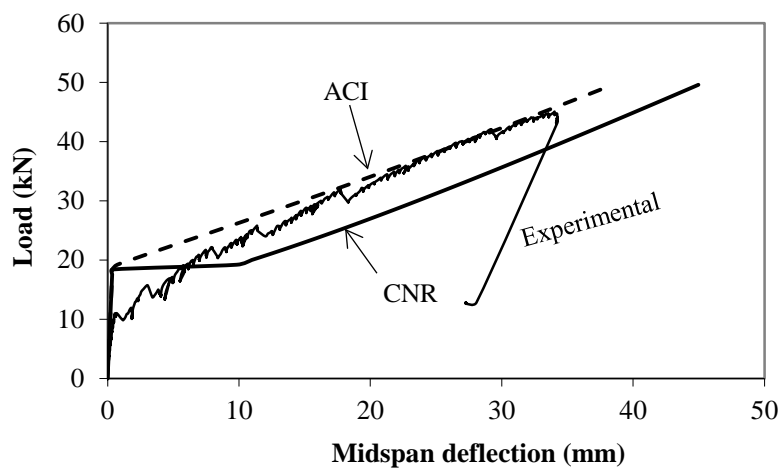
1 kN = 0.2248 kips; 1 mm = 0.0394 in
Fig. 11. Experimental and predicted deflections for slab CB-125–UO.
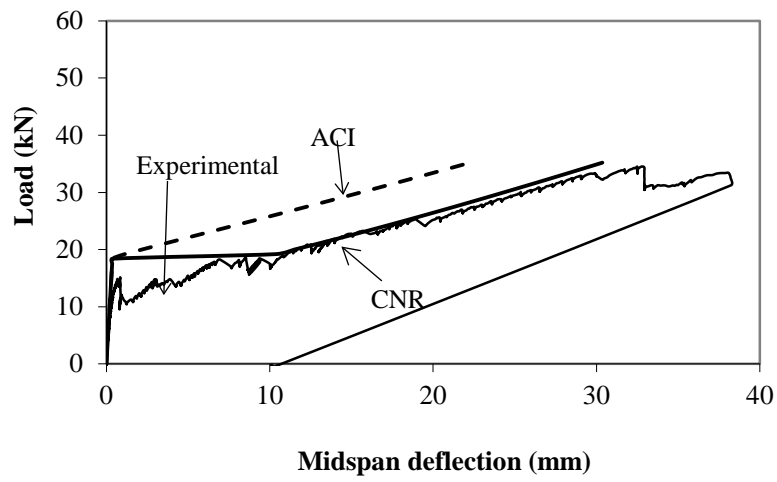
1 kN = 0.2248 kips; 1 mm = 0.0394 in

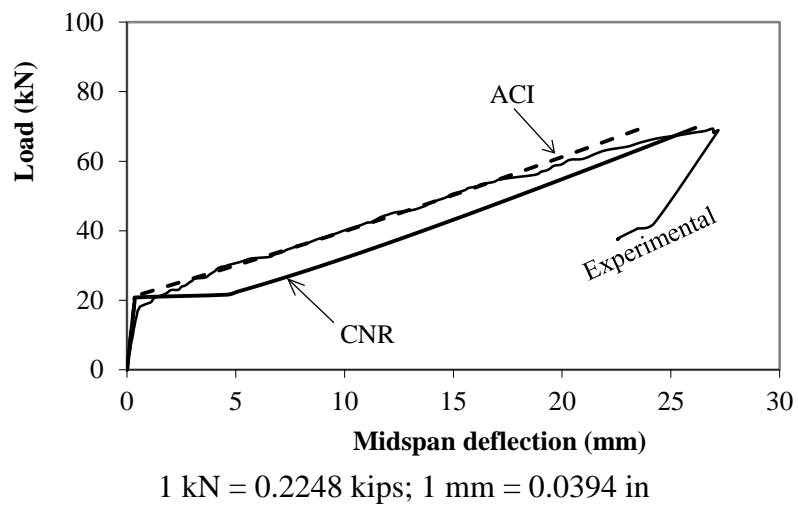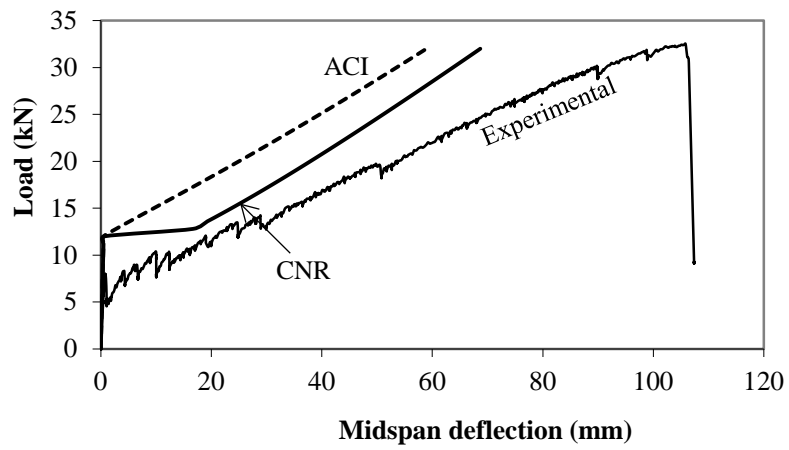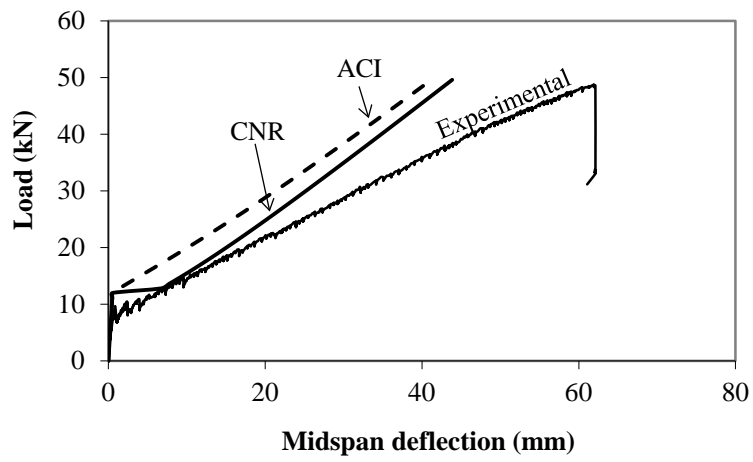**Fig. 12.** Experimental and predicted deflections for slab CB-125–UU.

Fig. 13. Experimental and predicted deflections for slab CB-125–OO.

1 kN = 0.2248 kips; 1 mm = 0.0394 in

Fig. 14. Experimental and predicted deflections for slab SB-125–U.

1 kN = 0.2248 kips; 1 mm = 0.0394 in
Fig. 15. Experimental and predicted deflections for slab SB-125–O.